Peer-reviewed version available at *Materials* **2019**, *12*, 3739; doi:10.3390/ma12223739

Article

The Effect of Co-Doping at the A-Site on the Structure and Oxide Ion Conductivity in $(Ba_{0.5-x}Sr_x)La_{0.5}InO_{3-\delta}$: A Molecular Dynamics Study

Kuk-Jin Hwang [1], Hae-Jin Hwang [2], Myung-Hyun Lee [1], Seong-Min Jeong [1,*], and Tae Ho Shin [1,*]

1 Energy & Environmental Division, Korea Institute of Ceramic Engineering and Technology, 101 Soho-ro, Jinju-si, Gyeongsangnam-do 52851, Korea; kjhwang@kicet.re.kr (K.-J.H.); mhlee@kicet.re.kr (M.-H.L.); smjeong@kicet.re.kr (S.-M.J.); ths@kicet.re.kr (T.H.S.)

2 School of Materials Science and Engineering, Inha University, 100 Inha-ro, Michuhol-gu, Incheon 22212, Korea; hjhwang@inha.ac.kr (H.-J.H.)

* Correspondence: smjeong@kicet.re.kr (S.-M.J.), ths@kicet.re.kr (T.H.S.)

Abstract: The molecular dynamics simulation has been used to investigate the structural and transport properties of $(Ba_{0.5-x}Sr_x)La_{0.5}InO_{3-\delta}$ (x=0, 0.1, 0.2) oxygen-ion conductor. The previous studies reported that the ionic conductivity of Ba-doped $LaInO_3$ decreases because Ba dopant forms narrow oxygen path in the lattice, which could hinder the diffusion of oxygen ion. In this study, we reveal the mechanism to improve the ionic conductivity by Ba and Sr co-doping on La site in $LaInO_3$ perovskite oxide. The results show that the ionic conductivity of $(Ba_{0.5-x}Sr_x)La_{0.5}InO_{3-\delta}$ increases with increasing numbers of Sr ions, which oxygen diffusion paths including Sr ion have larger critical radius than Ba ions. The RDF calculations showed the heights of peak in composition including Sr ions is lower and broaden, so oxygen ions moved easily into other oxygen sites.

Keywords: oxide ion conductivity; perovskite oxide; molecular dynamics simulation; ceramics electrolyte

1. Introduction

Ceramic ion conductors are important materials for application in solid oxide fuel cells (SOFCs), oxygen pumps, oxygen sensors due to its oxide ion conductivity and chemical and mechanical stability at high operating temperature [1-3]. The oxide ion conduction occurs via hopping mechanism through oxygen vacancies, which is generated the doping of low-valent cation to maintain the charge neutrality at the given composition. To achieve a high ionic conductivity, oxygen ion conductors must have large open space that allows high level of point defect disorder, and low migration enthalpy [4]. Some examples of such oxides are ZrO_2, CeO_2, Bi_2O_3 based oxide with fluorite structure, $LaGaO_3$ based perovskites, $Bi_4V_2O_{11}$ and $La_2Mo_2O_9$ based derivatives, $Ba_2In_2O_5$ derived perovskite, and brownmillerite like phases and pyrochlores [5].

Among them, fluorite-related structures such as yttria-stabilized zirconia (YSZ) show good performance as an oxide ion conductors at high temperatures (~0.1 $S{\cdot}cm^{-1}$ at 1273 K). However, it is well known that the electrical conductivity of YSZ decreases around 0.03 $S{\cdot}cm^{-1}$ at 1073 K [6]. Therefore, in most of the fluorite-related structures, high temperature is required for efficient operation.

To obtain the high ionic conductivity at intermediate temperature (873-1073 K), perovskite and related oxides have been extensively studied. ABO_3 perovskite oxides having a large number of oxygen vacancies can be introduced into the lattice by the substitution of cation A or B with lower valence cations. Many researchers have studied La-based ABO_3 perovskite as an electrolyte for

intermediate temperature SOFC (IT-SOFC) due to its high ionic conductivity and phase stability [7-11]. The perovskite oxide of the $La_{0.8}Sr_{0.2}Ga_{0.8}Mg_{0.2}O_{3-\delta}$ shows high oxide-ion conductivity, which is higher than that of the YSZs [12]. Therefore, many researches were conducted to utilize these electrolytes in the SOFC. On the other hand, doped $LaInO_3$ was introduced for electrolyte material: He et al. [13] studied the Sr doped $LaInO_3$ and Kim et al. [14] reported the Ba doped $LaInO_3$. However, these composites show low ionic conductivity than doped $LaGaO_3$. To improve the performance of $LaInO_3$, Kakinuma et al. [15] reported the co-doped $LaInO_3$, $(La_{0.5}Ba_{0.3}Sr_{0.2})InO_{2.75}$ showed very high conductivity, which was almost equal to $La_{0.8}Sr_{0.2}Ga_{0.8}Mg_{0.2}O_{3-\delta}$.

In previous studies, it was expected that the ionic conductivity of Ba-doped $LaInO_3$ increased with the formation of oxygen vacancies as the Ba ion was substituted [16]. However, it showed a maximum at 0.4 – 0.5 of Ba contents and decreased because Ba ion acts as a barrier of oxygen ion transport. Therefore, the aim of this study is to reveal the mechanism for improvement the ionic conductivity by Ba and Sr ions co-doping on La site in $LaInO_3$ using structural investigation method using molecular dynamics simulation.

2. Experimental and Simulation Methods

2.1. Experimental Method

The specimens of the $(Ba_{0.5-x}Sr_x)La_{0.5}InO_{3-\delta}$ (x = 0 – 0.2) were prepared through the conventional solid-state reaction method. The starting reagents used in this study were $La(NO_3)_3{\cdot}6H_2O$ (99%, Wako Chemical Co. Ltd., Japan), BaO (90%, Acros, US), $Sr(NO_3)_2{\cdot}6H_2O$ (99%, Sigma Aldrich, US) and In_2O_3 (99.99%, High Purity Chemicals Co. Ltd., Japan). The powders were mixed in a beaker with 100 mL of deionized water under magnetic stirring. This solution was dried and calcined at 673 K for 2 h, following by firing at 1773 K for 5 h for crystallization.

The crystalline phase of $(Ba_{0.5-x}Sr_x)La_{0.5}InO_{3-\delta}$ (x = 0 – 0.2) was identified using X-ray diffraction (XRD) on a X-ray diffractometer (D/max 2200V/PC, Rigaku, Japan), with Cu Kα radiation (λ = 1.5406 Å) produced at 40 kV and 200 mA to scan the diffraction angles (2θ) between 10 and 90° with a step size of 0.02° at 2θ per second. The diffraction results were refined to analyze their crystal structure, inter-ionic distances and lattice parameters by the Rietveld refinement method using the GSAS EXPGUI software package [17-18]. Crystallographic information file (CIF) for cubic space group Pm-3m was taken from Uchimoto et al. [19] with lattice parameters a = b = c = 4.17214 Å.

For the electrical conductivity measurements, these composites were prepared rectangular-shaped bars with a size of 3 mm × 3 mm × 10 mm. The platinum wires and platinum electrodes were formed by applying organic pastes (TR-7907, Tanaka Kinkinzoku Kogyo K. K., Japan) and firing at 1173 K to remove the organics. The conductivity were evaluated by using a general 4 terminal D.C. method and a custom jig with a Keithley 2400 Source Meter over a temperature range from 600 to 1273 K with steps of 100 K at a rate of 5 °C·min^{-1}.

2.2. Simulation Method

The interatomic potentials employed in this study were the Born model framework [20-22] consisting of a columbic term, a short range repulsion term and a dispersion term as follows:

$$U_{ij} = \frac{q_i q_j}{r_{ij}} + f_o(b_i + b_j)\exp\left[\frac{a_i + a_j - r_{ij}}{b_i - b_j}\right] - \frac{c_i c_j}{r_{ij}^6} \quad (1)$$

where q_i and q_j are the charges of two ions i and j, respectively. r_{ij} is the distance between i and j ions. f_0 is a constant for unit adaptation (=1kcal·mol^{-1}·Å^{-1}). The potential parameters a, b and c for each of the ions are shown in Table 1 [23, 24]. The simulation models consist of 200 unit cells with a total of 950 atoms. Table 1 shows the three models characterized with their oxide ion conduction pathway by Sr contents. The pathway depends on the arrangement of atoms at the A-site positions, and the three models with different amount of oxide ion pathway values were obtained by the manual arrangement of La, Sr and Ba ions.

Table 1. Interatomic potential parameters and configurations of oxide ion conduction pathway with different Sr ion contents for $(Ba_{0.5-x}Sr_x)La_{0.5}InO_{3-\delta}$.

Interatomic potential parameters					
	La	Ba	Sr	In	O
a (Å)	2.149	1.800	2.028	2.013	1.568
b (Å)	0.205	0.077	0.194	0.220	0.087
c $(kcal \cdot Å^6/mol)^{0.5}$	0	0	0	0	27

Configurations of oxide ion conduction pathway						
x	△LaLaIn	△LaBaIn	△LaSrIn	△BaSrIn	△SrSrIn	△BaBaIn
0	572	1256				572
0.1	572	964	292	172	8	392
0.2	572	716	540	284	68	220

All calculations were carried out using the MD simulation software LAMMPS (Sandia National Laboratory, USA) [25]. Newton's equation of motion was integrated for 1600 ps with a time step of 1 fs, after a relaxation step for 400 ps to remove the effect of the initial arrangement of oxygen vacancies. Each model with various compositions was simulated at temperatures from 873 K to 1273 K under a pressure of 1 bar. To derive the ionic conductivity, the mean square displacement (MSD) of oxygen ion was calculated according to

$$MSD(t) = \frac{1}{N}\sum_{i=0}^{N}(r(t) - r(0))^2 \quad (2)$$

where N is the total number of ions and r(t) is the position of an ion i at the time t. MSD has a relation to the diffusion coefficient as the Einstein relation

$$MSD(t) = 6Dt \quad (3)$$

where t is the time and D is the diffusion coefficient. The ionic conductivity was obtained from the diffusion coefficient according to the Nernst-Einstein equation

$$\sigma = \frac{q^2 ND}{fk_B TV} \quad (4)$$

where σ is ionic conductivity, kB is Boltzmann constant, T is temperature, f is Haven ratio, V is volume and q is the ion's charge. f had been calculated 0.69 for the perovskite structure [26].

The radial distribution function (RDF) was calculated to analyze the interaction between oxide ions and cation pairs using the following equation:

$$g(r) = \frac{dN/N}{dV/V} = \frac{V}{N}\frac{\langle N(r, \Delta r)\rangle}{4\pi r^2 \Delta r} \quad (5)$$

where V is the simulation cell volume, N is the total number, N(r, Δr) is the number of atom found within a spherical shell of r to r+Δr and the bracket represents a time average.

3. Results

Powder diffraction patterns of $(Ba_{0.5-x}Sr_x)La_{0.5}InO_{3-\delta}$ (x=0, 0.1, and 0.2) sintered at 1773 K are shown in Figure 1(a). A single phase was observed in all compositions and the X-ray diffraction patterns could be indexed as a simple cubic structure, indicating that 20 at.% of barium on A-site could be substituted by strontium. It has been reported that LaInO3 exhibits an orthorhombic phase at room temperature and the cubic phase is formed by doping of barium on lanthanum-site; as the doping content of barium increased in the $La_{1-x}Ba_xInO_{3-\delta}$ system, a mixture of cubic and orthorhombic phases was produced for the compositions of x = 0.1 - 0.3 and the single cubic phase was formed of the compositions of x = 0.4 - 0.8 [14]. According to the study on the lattice parameter

Preprints (www.preprints.org) | NOT PEER-REVIEWED | Posted: 16 October 2019 doi:10.20944/preprints201910.0177.v1

Peer-reviewed version available at Materials 2019, 12, 3739; doi:10.3390/ma12223739

in the $La_{1-x}Sr_xInO_{3-\delta}$ system, however, the solubility limit of strontium on A-site in $LaInO_3$ was reported as about x = 0.1 although the ionic radius of strontium is similar to that of lanthanum [13]. And Ruiz-Trejo et al. [27] suggested that the best dopant was strontium on lanthanum-site by the calculating the energy of alkaline-earth ions into the lanthanum-site, indicating that the soluble amount of dopant on A-site in $LaInO_3$ may be independent to the ionic radius or the energy of solution. It is interesting that the substituted amount of strontium was at least 20 at.% in the $(Ba_{0.5-x}Sr_x)La_{0.5}InO_{3-\delta}$ system whereas it was about 10 at.% in the $La_{1-x}Sr_xInO_{3-\delta}$ system. The existence of barium might enhance the substituted amount of strontium. Using this XRD results, crystal structure was investigated using Rietveld refinement as shown in Figure 1(b).

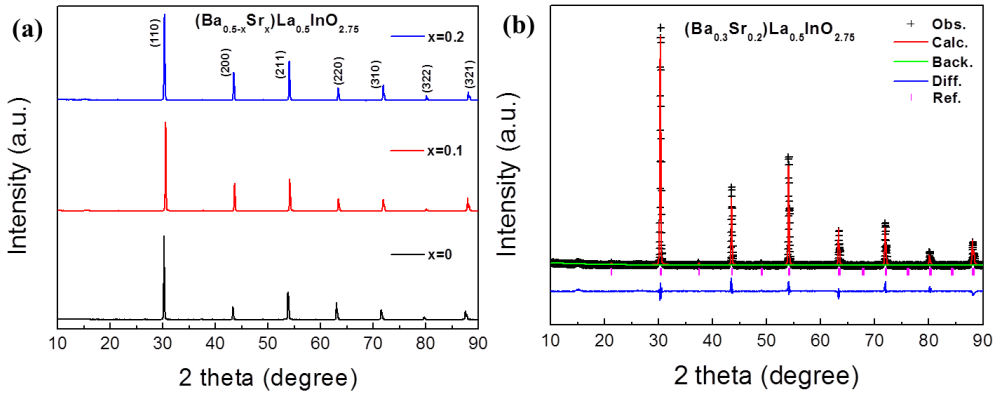

Figure 1. (a) XRD spectra of $(Ba_{0.5-x}Sr_x)La_{0.5}InO_{3-\delta}$ (x=0, 0.1, and 0.2) sintered at 1773 K for 5 h. (b) Rietveld refinement of the $(Ba_{0.3}Sr_{0.2})La_{0.5}InO_{3-\delta}$. The plus mark and red line represent the experimental and calculated intensities, respectively; the blue line is the difference between them. Tick marks (magenta) indicate the positions of Bragg peaks.

Figure 2 shows the lattice parameters of $(Ba_{0.5-x}Sr_x)La_{0.5}InO_{3-\delta}$ as a function of Sr content. The lattice parameters decrease with increasing Sr content, because a Sr ion has a smaller ionic radius than Ba ions. Also, as the amount of Sr ion increase, the lattice constants decrease continuously, suggesting that Ba and Sr ions have been replaced by La ions and no secondary phase is formed. It is also indicated that oxygen vacancies are generated for charge compensation as Ba ions and Sr ions are substituted for La ion sites. The calculated lattice parameters were ~0.3 % lower than the experimental values, indicating that the interatomic potentials used in this study were reasonably accurate.

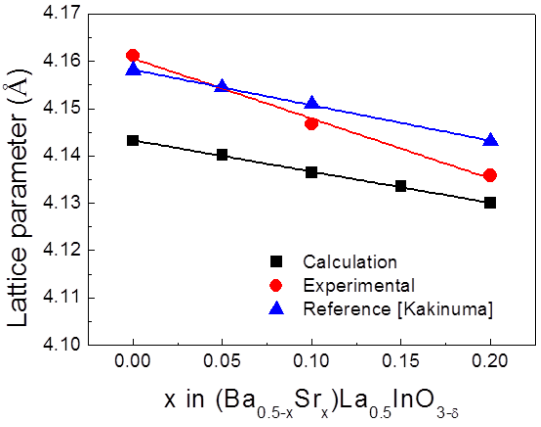

Figure 2. Lattice parameters of $(Ba_{0.5-x}Sr_x)La_{0.5}InO_{3-\delta}$ as a function of Sr content compared with experimental and reference values.

Figure 3(a) and (b) show the ternary oxides with ABO_3 cubic perovskite structure and oxide ion pathway of oxygen octahedron site in the perovskite structure, which is consisted of four A-site ions

and two B-site ions. In the perovskite structure, oxide ion can be moved through the oxygen pathway as shown in Figure 3(b), so we investigated the diffusion behavior of all oxide ions. Figure 3(c) shows the calculated MSDs of each ion in Sr contents at 1073 K. One of the main purposes of MSD analysis is the extraction of the diffusion coefficient value from the simulation [28]. In Figure 3(c), the MSDs for all the ions in the $(Ba_{0.3}Sr_{0.2})La_{0.5}InO_{3-\delta}$ composite are presented at 1073 K. It clearly shows that the MSD of oxygen ions continuously increases with time. However, the MSDs of cations show a constant value and there is no cation diffusion in the perovskite oxides. These results shows that $(Ba_{0.5-x}Sr_x)La_{0.5}InO_{3-\delta}$ is the pure oxide ion conductor [15]. In Figure 3(d), we focused on the MSD of oxygen ions as the Sr ion contents, which clearly demonstrates that the oxygen ion transport property is increased as the amount of Sr ion increase.

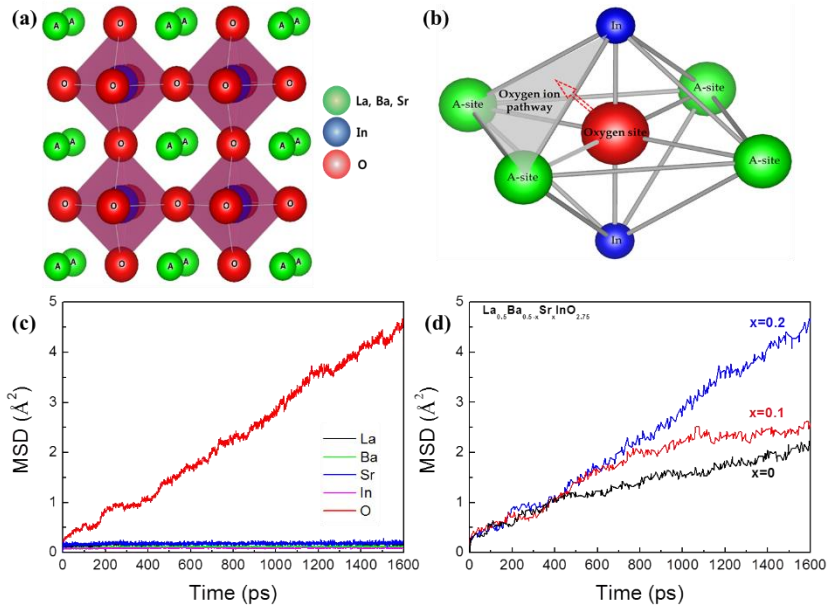

Figure 3. (a) Typical ABO_3 perovskite structure, (b) Schematic diagram of oxygen octahedral site and oxygen path way, (c) MSD of each ions in $(Ba_{0.3}Sr_{0.2})La_{0.5}InO_{3-\delta}$ (d) MSD of oxygen ions in Sr contents at 1073 K.

Figure 4 shows an Arrhenius plot of the ionic conductivity with experimental values at the temperature ranges from 873 K to 1273 K. The calculated ionic conductivity for $(Ba_{0.5-x}Sr_x)La_{0.5}InO_{3-\delta}$ was lower than experimental data for all compositions. The interatomic potential used for this research is empirical potential. It is difficult to exactly reproduce the experimental values due to the limitation, so there is a little error between the calculated and experimental values. The ionic conductivity, σ, is represented by three terms, i.e. carrier concentration, C, carrier charge, Ze, where Z is the valence and e is the electronic charge, and carrier mobility, μ.

$$\sigma = CZe\mu \quad (6)$$

In this study, all the compositions have the same number of carrier: oxygen ions, but higher ionic conductivity was obtained on higher contents of Sr ions. In order to investigate the effect of Sr ion substitution on the ionic conductivity and carrier mobility increase, the tolerance factor and lattice free volume was considered.

Preprints (www.preprints.org) | NOT PEER-REVIEWED | Posted: 16 October 2019 doi:10.20944/preprints201910.0177.v1

Peer-reviewed version available at Materials 2019, 12, 3739; doi:10.3390/ma12223739

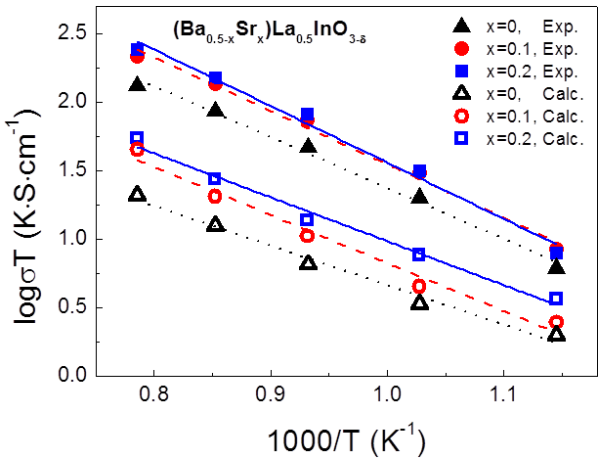

Figure 4. Arrhenius plots for the ionic conductivity of $(Ba_{0.5-x}Sr_x)La_{0.5}InO_{3-\delta}$ at 873-1273 K.

For the understanding about the oxygen-ion conduction in the perovskite-structured oxides, several parameters, such as tolerance factor, lattice free volume and critical radius, influenced on the oxygen-ion conductivity [29-31]. Figure 5 shows the relationship between ionic conductivity, lattice free volume and tolerance factor depending on the amount of Sr ions. The lattice free-volume was defined as the difference between the unit cell volume and the summed volume occupied by all constituent ions. As the free volume increases, the lattice spacing increases and the carrier ions can be moved easily, therefore ionic conductivity increases. Figure 5 shows that the lattice free volume of $(Ba_{0.5-x}Sr_x)La_{0.5}InO_{3-\delta}$ decreased with increasing Sr content and ionic conductivity increased. Also, the Goldschmidt tolerance factor in followed equation, decreased with increasing Sr ion.

$$G_t = (r_A + r_O)/\left(\sqrt{2}(r_B + r_O)\right) \quad (7)$$

Where, r_A, r_B and r_O are a ionic radius of A, B cations and oxygen ion. The Goldschmidt tolerance factor can predict the structural stability depending on the degree of distortion of the BO_6 octahedron in perovskite structure. The ideal cubic structure has a 1 and the further the value deviates from 1, the lower the structural symmetry and the lower the conductivity too.

In general, it is known that the better the structural symmetry, the closer the Goldschmidt tolerance factor is to 1, the higher the ionic conductivity. However, in this study, the opposite result was obtained. In Figure 1, the XRD results showed cubic structure in all compositions and there is no effect of BO_6 distortion on ionic conductivity.

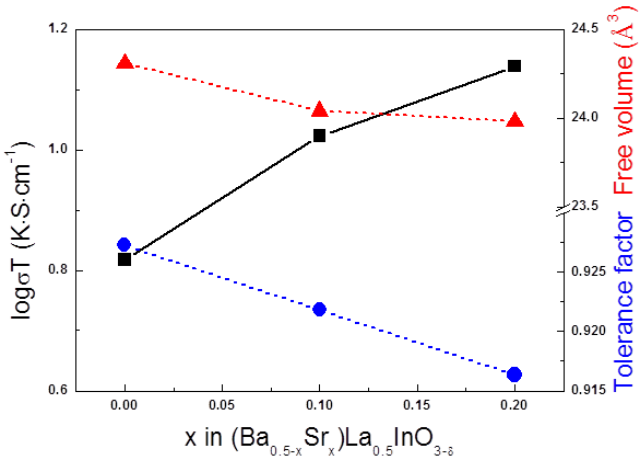

Figure 5. Ionic conductivity and tolerance factor (blue), free volume (red) of $(Ba_{0.5-x}Sr_x)La_{0.5}InO_{3-\delta}$ at 1073 K.

Table 2 shows the critical radius of oxygen ion pathway with different Sr ion contents in $(Ba_{0.5-x}Sr_x)La_{0.5}InO_{3-\delta}$. The critical radius was defined as the critical size of the triangle formed by two A-site cations and one B-site cation where oxygen-ions move into adjacent oxygen vacancies. As the critical radius is large, the ionic conductivity shows high value. As shown in Table 2 the critical radius is larger in the pathway with Sr ion rather than with Ba ion. As the amount of Sr ion increased, the critical radius increased and the tolerance factor and lattice free volume decreased. When La ion sites are substituted with low-valent cation having large ionic radius, the ionic conductivity depends on the critical radius among the various factors in $LaInO_3$ perovskite. These result will be useful for predicting the ionic conduction properties when the synthesis of perovskite oxides.

Table 2 The critical radius of oxygen ion pathway with different Sr ion contents in $(Ba_{0.5-x}Sr_x)La_{0.5}InO_{3-\delta}$.

	△LLI	**△LBI**	**△BBI**	**△LSI**	**△SSI**	**△BSI**
x=0	0.993	0.925	0.832			
x=0.1	0.998	0.918	0.829	0.962	0.967	0.874
x=0.2	0.996	0.906	0.832	0.954	0.95	0.883

Figure 6 shows the probability of the oxygen ion transport according to the oxygen ion pathway, Nm/Np represents the amount of movement of the oxygen ions per adjacent oxygen ion pair by break the A-O ionic bonds. The bonding energies of O-Sr and O-Ba were -1664 and -1469 kJ/mol, respectively, and more energy would be required to break an O-Sr compared O-Ba bonds. Therefore, the oxide ion can be easily moved through the oxygen pathway including Ba ions. However, in all compositions, the amount of oxygen ions moving through the △LLI pathway occupies the greatest proportion. The ratio of passing through △LBI was smaller than that of △LSI, and it was confirmed that the critical radius is a crucial factor to reveal the oxygen transport property in doped $LaInO_3$ perovskite structure.

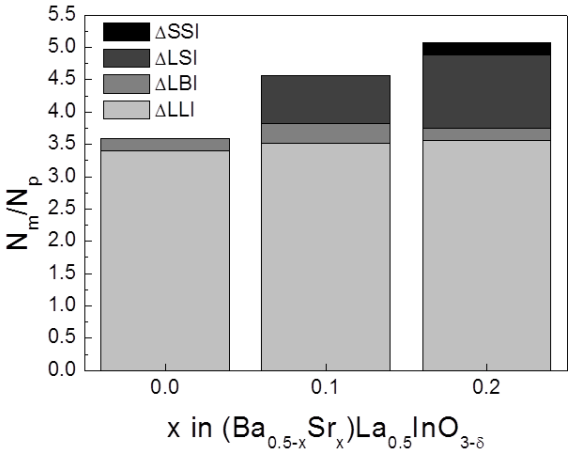

Figure 6. Probability of oxygen ion migration through pathway in $(Ba_{0.5-x}Sr_x)La_{0.5}InO_{3-\delta}$ at 1073 K.

To discover the structural difference between the Sr doping and un-doping composition, the interionic distance between particular ions and oxygen ions were analyzed using the RDF function. Figure 7 (a), (b) and (c) show RDF curves for the ionic pairs of La-O, In-O and O-O in $(Ba_{0.5-x}Sr_x)La_{0.5}InO_{3-\delta}$. In all compositions, there were no significant differences however, as the Sr ion is substituted, the peak of RDF is lower and broadens which suggests that the doping composition is a distorted form derived from the un-doped composition [32-33]. In Figure 7(c) indicates that the oxygen ion do not exists in the original position and substitution of Sr ion to A sites makes it easy to move the oxygen ion because it permits the amount of oxygen vacancies in neighboring O ions to be

estimated. Because the higher peak intensity of the O–O pair is indicative of a smaller number of oxygen-vacancy pairs in the lattice structure, the un-doped composite was estimated to have less oxygen-vacancy pairs than the Sr doped composite. This means that more conduction paths are available in the Sr doped composite, so that a higher ionic conductivity would be expected. This study suggests that to achieve a high ionic conductivity in doped $LaInO_3$, the critical radius should be larger by substitution of cations.

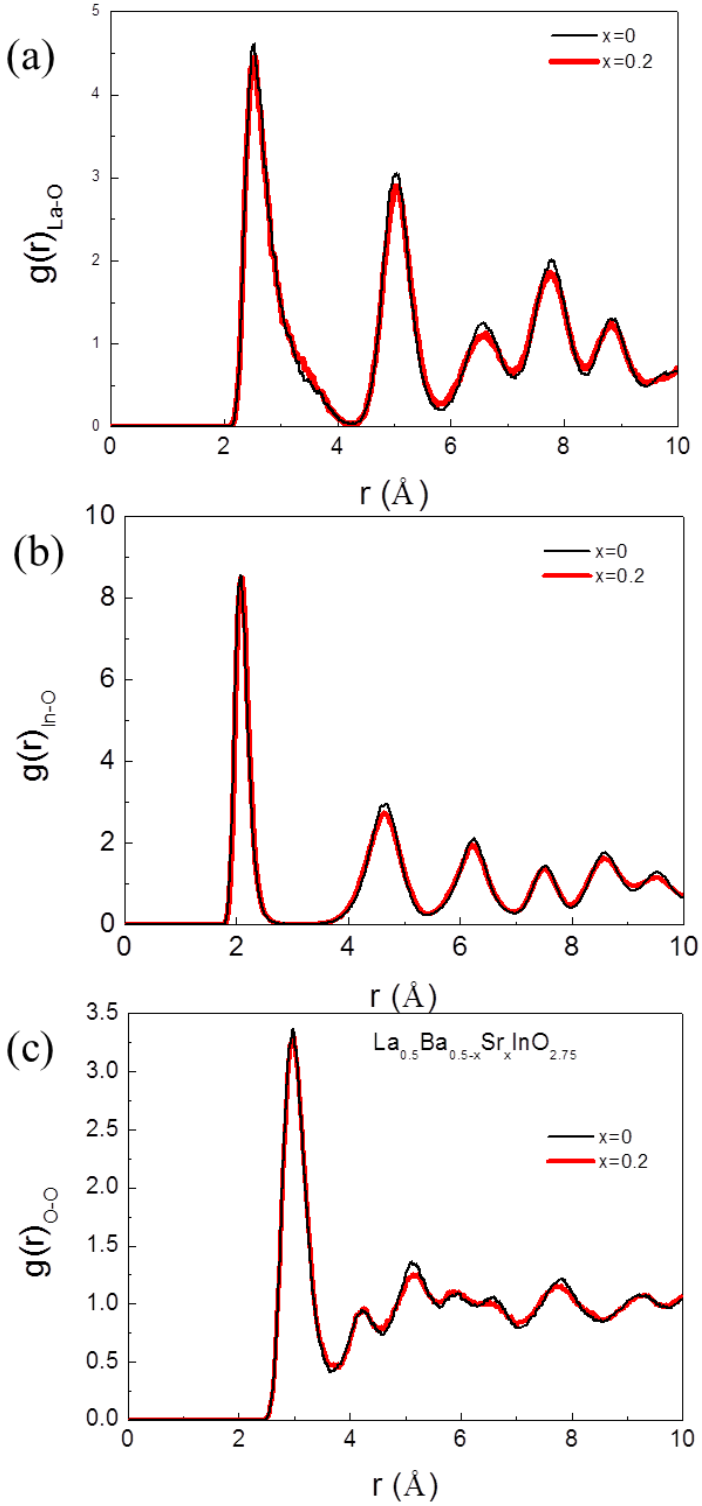

Figure 7. RDF (a) La-O ions, (b) In-O ions and (c) O-O ions in $(Ba_{0.5-x}Sr_x)La_{0.5}InO_{3-\delta}$ at 1073 K.

4. Conclusions

In this study, the oxygen ion conductivity and conduction mechanism of Ba and Sr doped $LaInO_3$ were analyzed using molecular dynamics simulation. The $(Ba_{0.5-x}Sr_x)La_{0.5}InO_{3-\delta}$ composites are verified the oxygen ion conductor by calculation the MSD and increasing Sr contents, the MSD of oxygen ion and ionic conductivity increased too. As the substitution of Sr ion with small ionic radius to Ba ion site, reduced the tolerance factor and lattice free volume, but critical radius increased, therefore, the critical radius is a dominant factor in doped $LaInO_3$ perovskite. As a result of RDF calculation, the oxygen ion tends to deviated from the original oxygen ion site in doped Sr ion composition. To achieve high ionic conductivity, the oxygen pathway should have large critical radius in doped $LaInO_3$.

Author Contributions: Conceptualization, H.-J.J and S.-M.J.; Data Curation, K.-J.H.; Project Administration, M.-H.L. and T.H.S.; Writing—Original Draft Preparation, K.-J.H.; Writing—Review and Editing, S.-M.J. and T.H.S.

Funding: This work was supported by the Technology Innovation Program (no. 10063427) and International R&D Program (grant no. P0004433) by the Ministry of Trade, Industry & Energy (MOTIE) of the Republic of Korea. And this work was supported by the Korea Institute of Energy Technology Evaluation and Planning (KETEP) and the Ministry of Trade, Industry & Energy (MOTIE) of the Republic of Korea (No. 20182010600400)

Conflicts of Interest: The authors declare no conflict of interest.

References

1. Fergus, J.W. Electrolytes for solid oxide fuel cells. *J. Power Sources.* **2006**, *162*, 30-40. https://doi.org/10.1016/j.jpowsour.2006.06.062.
2. Ramamoorthy, R.; Dutta, P.K.; Akbar, S.K. Oxygen Sensors: Materials, methods, designs and applications. *J. Mater. Sci.* **2003**, *38*, 4271-4282. https://doi.org/10.1023/A:1026370729205.
3. Badwal, S.P.S.; Drennan, J. Yttria-zirconia: effect of microstructure on conductivity, *J. Mater. Sci.* **1987**, *22*, 3231-3239. https://doi.org/10.1007/BF01161187.
4. Xia, C. Electrolytes, in Solid oxide fuel cells materials properties and performance; Fergus, J.W.; Hui, R.; Li, X.; Wilkinson, D.P.; Zhang, J. Eds.; CRC Press Taylor & Francis Group, FL, USA, 2009; pp. 3-5. https://doi.org/10.1201/9781420088847.
5. Kharton, V.V.; Marques, F.M.B.; Atkinson, A. Transport properties of solid oxide electrolyte ceramics: a brief review. *Solid State Ion.* **2004,** *174*, 135-149. https://doi.org/10.1016/j.ssi.2004.06.015.
6. Yamamoto, O.; Arati, Y.; Takeda, Y.; Imanishi, N.; Mizutani, Y.; Kawai, M.; Nakamura, Y. Electrical conductivity of stabilized zirconia with ytterbia and scandia. *Solid State Ion.* **1995,** *79*, 137-142. https://doi.org/10.1016/0167-2738(95)00044-7.
7. Wang, S.; Jiang, Y.; Zhang, Y.; Yan, J.; Li, W. Promoting effect of YSZ on the electrochemical performance of YSZ+LSM composite electrodes. *Solid State Ion.* **1998,** *113-115*, 291-303. https://doi.org/10.1016/S0167-2738(98)00379-8.
8. Lybye, D.; Poulsen, F.W.; Mogensen, M. Conductivity of A- and B-site doped $LaAlO_3$, $LaGaO_3$, $LaScO_3$ and $LaInO_3$ perovskites. *Solid State Ion.* **2000,** *128*, 91-103. https://doi.org/10.1016/S0167-2738(99)00337-9.
9. Huang, P.; Petric, A. Superior oxygen ion conductivity of lanthanum gallate doped with strontium and magnesium. *J. Electrochem. Soc.* **1996**, *143*, 1644-1648. https://doi.org/10.1149/1.1836692.
10. Nomura, K.; Tanase, S. Electrical conduction behavior in $(La_{0.9}Sr_{0.1})M^{III}O_{3-\delta}$ (M^{III} = Al, Ga, Sc, In, and Lu) perovskites. *Solid State Ion.* **1997,** *98*, 229-236. https://doi.org/10.1016/S0167-2738(97)00101-X.
11. Nomura, K.; Takeuchi, T.; Tanase, S.; Kageyama, H.; Tanimoto, K.; Miyazaki, Y. Proton conduction in $(La_{0.9}Sr_{0.1})M^{III}O_{3-\delta}$ (M^{III} = Al, Ga, Sc, In, and Lu) perovskites. *Solid State Ion.* **2002,** *154-155*, 647-652. https://doi.org/10.1016/S0167-2738(02)00512-X.
12. Ishihara, T.; Matsuda, H.; Takita, Y. Doped $LaGaO_3$ perovskite type oxide as a new oxide ionic conductor. *J. Am. Chem. Soc.* **1994**, *116*, 3801-3803. https://doi.org/10.1021/ja00088a016.
13. He, H.; Huang, X.; Chen, L. Sr-doped $LaInO_3$ and its possible application in a single layer SOFC. *Solid State Ion.* **2000,** *130*, 183-193. https://doi.org/10.1016/S0167-2738(00)00666-4.
14. Kim, H.; Lee, K.; Kim, S.; Lee, H. Electrical conduction behavior of BaO-doped $LaInO_3$ perovskite oxide. *Jpn. J. Appl. Phys.* **2006**, *45*, 872-874. https://doi.org/10.1143/JJAP.45.872.

15. Kakinuma, K.; Arisaka, T.; Yamamura, H.; Atake, T. Solid oxide fuel cell using ($Ba_{0.3}Sr_{0.2}La_{0.5}$)$InO_{2.75}$ electrolyte. *Solid State Ion.* **2004,** *175*, 139-143. https://doi.org/10.1016/j.ssi.2004.09.030.
16. Byeon, D.; Jeong, S.; Hwang, K.; Yoon, M.; Hwang, H.; Kim, S.; Lee, H. Oxide ion diffusion in Ba-doped LaInO3 perovskite: A molecular dynamics study. *J. Power Sources.* **2013**, *222*, 282-287. https://doi.org/10.1016/j.jpowsour.2012.08.091.
17. Larson, A.C.; Von Dreele, R.B. General structure analysis system (GSAS). Los Alamos National Laboratory Report LAUR **2004,** 86-748.
18. Toby, B.H. EXPGUI, A graphical user interface for GSAS. *J. Appl. Cryst.* **2001**, *34*, 210-213. https://doi.org/10.1107/S0021889801002242.
19. Uchimoto, Y.; Takagi, H.; Yao, T.; Ozawa, N.; Inagaki, T.: Yoshida, H. EXAFS study of crystal structures of (Ba1-xLax)2In2O5+x and their oxide ion conductivity. *J. Sync. Rad.* **2001**, *8*, 857-859. https://doi.org/10.1107/S090904950002094X.
20. Fumi, F.G.; Tosi, M.P. Ionic sizes and born repulsive parameters in the NaCl-type alkali halides-I: the Huggins-Mayer and pauling forms. *J. Phys. Chem. Solids.* **1964**, *25*, 31-43. https://doi.org/10.1016/0022-3697(64)90159-3.
21. Tosi, M.P.; Fumi, F.G. Ionic sizes and born repulsive parameters in the NaCl-type alkali halides-II: the generalized Huggins-Mayer form. *J. Phys. Chem. Solids.* **1964**, *25*, 45-52. https://doi.org/10.1016/0022-3697(64)90160-X.
22. Buckingham, R.A. The classical equation of state of gaseous helium, neon and argon. *Proc. R. Soc. Lond. A. Math. Phys. Sci.* **1938**, *168*, 264. https://doi.org/10.1098/rspa.1938.0173.
23. Yamamura, Y.; Ihara, C.; Kawasaki, S.; Sakai, H.; Suzuki, K.; Takami, S.; Kubo, M.; Miyamoto, A. Materials design of perovskite-based oxygen ion conductor by molecular dynamics method. *Solid State Ion.* **2003,** *160*, 93-101. https://doi.org/10.1016/S0167-2738(03)00154-1.
24. Tamai, Y.; Kawamoto, Y. Molecular dynamics simulation of permanet densification of fluorozirconate glass. *Chem. Phys. Lett.* **1999**, *302*, 15-19. https://doi.org/10.1016/S0009-2614(99)00115-3.
25. Plimpton, S. Fast parallel algorithms for short-range molecular dynamics. *J. Comput. Phys.* **1995**, *117*, 1-19. https://doi.org/10.1006/jcph.1995.1039.
26. Ishigaki, T.; Yamauchi, S.; Kishio, K.; Mizusaki, J.; Fueki, K. Diffusion of oxide ion vacancies in perovskite-type oxides. *J. Solid State Chem.* **1998**, *73*, 179-187. https://doi.org/10.1016/0022-4596(88)90067-9.
27. Ruiz-Trejo, E.; Tavizon, G.; Arroyo-Landeros, A. Structure, point defects and ion migration in $LaInO_3$. *J. Phys. Chem. Solids*. **2003**, *64*, 515-521. https://dor.org/10.1016/S0022-3697(02)00358-X.
28. Islam, M.S.; Cherry, M.; Catlow, C.R.A. Oxygen diffusion in $LaMnO_3$ and $LaCoO_3$ perovskite-type oxides: A molecular dynamics study. *J. Solid State Chem*. **1996**, *124*, 230-237. https://doi.org/10.1006/jssc.1996.0231.
29. Goldschmidt, V.M. Die Gesetze Der Krystallochemie. *Naturwissenschaften* **1926**, *14*, 477-485. https://doi.org/10.1007/BF01507527.
30. Cook, R.L.; Sammells, A.F. On the systematic selection of perovskite solid electrolytes for intermediate temperature fuel cells. *Solid State Ion.* **1991**, *45*, 311-321. https://doi.org/10.1016/0167-2738(91)90167-A.
31. Kilner, J.A.; Brook, R.J. A study of oxygen ion conductivity in doped non-stoichiometric oxides. *Solid State Ion.* **1982,** *6*, 237-252. https://doi.org/10.1016/0167-2738(82)90045-5.
32. Clarke, A.S.; Jonsson, H. Structural changes accompanying densification of random hard-sphere packings. *Phys. Rev. E*, **1993**, *47*, 3975-3984. https://doi.org/10.1103/PhysRevE.47.3975.
33. Fabris, S.; Paxton, A.T.; Finnis, M.W. A stabilization mechanism of zirconia based on oxygen vacancies only. *Acta Mater.* **2002**, *50*, 5171-5178. https://doi.org/10.1016/S1359-6454(02)00385-3.